Chinese Chemical Letters 34 (2023) 107898

Contents lists available at ScienceDirect

Chinese Chemical Letters

journal homepage: www.elsevier.com/locate/cclet

Eliminating crystal water enables enhanced sodium storage performance in an oxalate-phosphate cathode material

Kena Sun[a], Huiwu Long[b], Xiaowu Jie[a,*], Huangxu Li[b,*]

[a] BGRIMM Technology Group, Beijing 100160, China
[b] Department of Chemistry, City University of Hong Kong, Hong Kong 999077, China

ARTICLE INFO

Article history:
Received 8 August 2022
Revised 24 September 2022
Accepted 12 October 2022
Available online 14 October 2022

Keywords:
V-based materials
Cathode
Energy storage
Crystal water
Battery

ABSTRACT

The oxalate-phosphate polyanion-mixed cathode materials are promising for sodium-ion batteries (SIBs) due to their unique open-framework structures and high voltage property. However, materials of this type generally contain crystal water molecules in the lattice frameworks, which may affect their energy storage properties. This work aims to disclose the impacts of crystal water on physiochemical and electrochemical properties of $Na_2(VO)_2(HPO_4)_2(C_2O_4)\cdot 2H_2O$ (NVPC-W). It shows that the water molecules can be eliminated by vacuum drying at 150 °C. The elimination of water molecules does not change the crystal phase of the material, while the obtained $Na_2(VO)_2(HPO_4)_2(C_2O_4)$ (NVPC) exhibits significant improvements in cycling stability, Coulombic efficiency, as well as rate performances. Kinetics analysis indicates that the existence of lattice water molecules hinders sodium-ion diffusion and promotes the degradation of electrodes. We believe the findings can help to develop high-performance cathode materials.

© 2023 Published by Elsevier B.V. on behalf of Chinese Chemical Society and Institute of Materia Medica, Chinese Academy of Medical Sciences.

Compared to the well-studied lithium-ion batteries (LIBs), sodium–ion batteries (SIBs) have been proposed as a better choice for large scale energy storage due to the abundant sodium resources and low cost [1–3]. Over the past decades, extensive efforts have been made to explore high performance electrode materials for sodium storage, and thus promote the practical applications of SIBs [4–6]. However, developing an ideal cathode material with high energy density, long lifespan, good rate capability, and high safety is still challenging.

As a main category of cathode materials, the polyanion-type compounds (PTCs) show great flexibility in crystal structure and composition for researchers to explore high performance materials [7–9]. The diverse polyanions and different connecting manners have led to the discovery of numerous PTCs for sodium storage, such as $NaFePO_4$ [10], $Na_2MP_2O_7$ (M: transition metals) [11,12], $Na_xM_IM_{II}(PO_4)_3$ [13–17]. Additionally, different anion groups can also be combined together to generate polyanion-mixed compounds, including $Na_3V_2(PO_4)_2F_3$ [18,19], $Na_4M_3(PO_4)_2(P_2O_7)$ [20,21], $Na_3V(PO_3)_3N$ [22], *etc.* Recently, the oxalate-phosphate polyanion-mixed materials, such as $Na_2[(VOHPO_4)_2(C_2O_4)]\cdot 2H_2O$ [23], $Li_2(VO)_2(HPO_4)_2(C_2O_4)\cdot 6H_2O$ [24] and $K_2[(VO)_2(HPO_4)_2(C_2O_4)]\cdot 4.5H_2O$ [25], have emerged as an attractive materials family. The materials demonstrate distinctive features for alkali-ion storage. Firstly, the strong electronegativity of (C_2O_4)-(PO_4) endows high voltage property of the materials. Secondly, the open-framework structure allows facile charge carrier migration. Notably, the oxalate-phosphate materials can be synthesized at low-temperature through wet-chemical approaches, which avoids high temperature calcination process and makes it easier to control morphology. One key issue is the oxalate-phosphate materials show low cycling stability and poor rate performance, which is imperative to be addressed.

Carbon coating, ion-doping, hierarchical structure construction, etc. are general strategies to improve electrochemical performance of PTCs [26–28]. Considering that most of the reported oxalate-phosphate materials contains crystal water, which commonly show negative impacts on organic battery systems [29], herein, we try to eliminate the crystal water in the typical oxalate-phosphate material $Na_2(VO)_2(HPO_4)_2(C_2O_4)\cdot 2H_2O$ (NVPC-W) and investigate the impacts of crystal water on material crystal structure, morphology, and electrochemical performance. It is found that the two water molecules can almost be fully removed and the elimination of water molecules does not change the crystal phase of the material. While the obtained $Na_2(VO)_2(HPO_4)_2(C_2O_4)$ (NVPC) exhibits significant improvements in cycling stability, Coulombic efficiency, as well as rate performances. Kinetics analysis has been employed to disclose the underlying mechanism. The discoveries deepen our understanding about the effects of crystal water and should be

* Corresponding authors.
E-mail addresses: jiexiaowu002@163.com (X. Jie), huangxuli2-c@my.cityu.edu.hk (H. Li).

https://doi.org/10.1016/j.cclet.2022.107898
1001-8417/© 2023 Published by Elsevier B.V. on behalf of Chinese Chemical Society and Institute of Materia Medica, Chinese Academy of Medical Sciences.

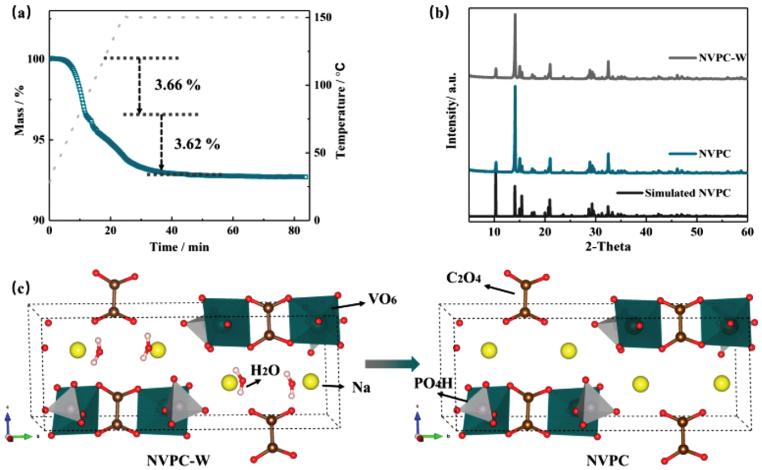

Fig. 1. Crystal structure of the NVPC-W and NVPC materials. (a) TGA curve and temperature curve of the NVPC-W material under Ar atmosphere. The TGA was carried out from room-temperature to 150 °C with a heating rate of 5 °C/min and kept at 150 °C for 1 h. (b) XRD patterns of the pristine NVPC-W and the NVPC. (c) Schematic illustration of the crystal structure of NVPC-W and NVPC.

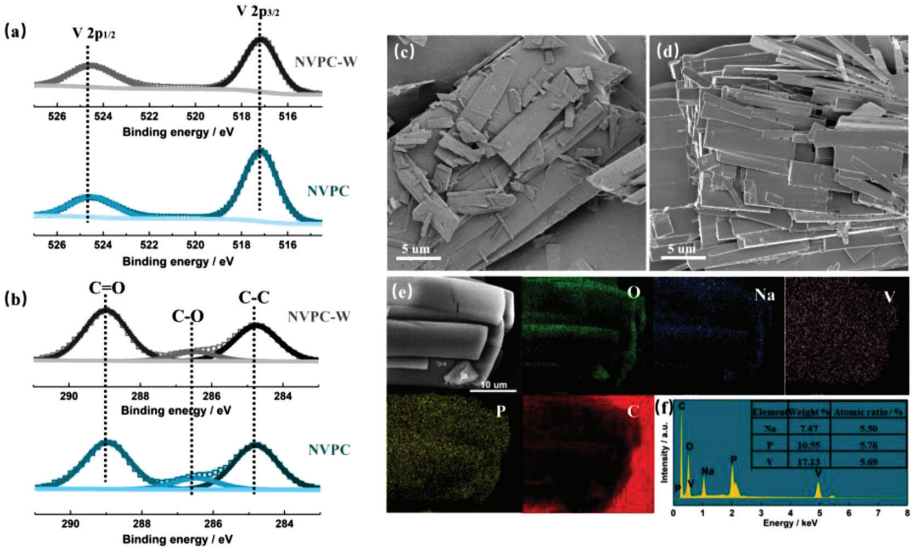

Fig. 2. Physiochemical properties of the materials. The XPS spectra of (a) V 2p and (b) C 1s. SEM images of (c) NVPC-W and (d) NVPC. (e) Elemental mapping images of O, Na, V, P, C and (f) the energy dispersive spectrometer (EDS) of NVPC.

helpful to develop advanced oxalate-phosphate electrode materials.

According to previous reports, the pristine NVPC-W that synthesized by hydrothermal method contains two crystal water molecules per formula [30]. The existence of crystal water, which may trigger unfavorable side reactions, is commonly deleterious for electrode materials, especially in organic electrolyte [31,32]. High temperature treatment can remove the crystal water, but it may also destroy the original crystal phase [33]. The possibility of eliminating crystal water has been primarily studied by Thermogravimetric analysis (TGA) and X-ray diffraction (XRD). TGA test under Ar shows a two–step water molecules extraction process. The first weight loss of 3.66% can be assigned to one water molecule extraction, and the second weight loss of 3.62% indicates extraction of the other water molecule (Fig. 1a). So, the two water molecules can be fully extracted from the lattice at 150 °C. To check the crystal phase evolution, NVPC-W was put into an oven at 150 °C under vacuum overnight to obtain anhydrous NVPC. XRD shows that the crystal phase of NVPC has no changes compared to pristine NVPC-W (Fig. 1b). Both of the NVPC-W and NVPC can be indexed to a monoclinic phase (S.G.: $P2_1$) [30,34]. Crystal phase of the materials are schematically illustrated. As shown in Fig. 1c, the materials possess a layered structure, which is distinctive as most PTCs generally present a three-dimensional framework structure. In detail, the [$VOHPO_4$] infinite chains along *a*–axis direction is constructed by corner-shared VO_6 octahedra and PO_4H tetrahedron. And the (C_2O_4) groups links these [$VOHPO_4$] chains along *b*–axis direction. Sodium-ions and crystal water molecules reside in the vacancy space. Since no significant crystal phase change is observed, the extraction of crystal water in NVPC-W can be a topologic process, which is consistent with previous reports [30].

After confirming the crystal phases, the impacts of the crystal water removal on chemical bonding and morphologies of the materials were then investigated. Chemical states and bonding structure of the NVPC-W and NVPC were probed by X–ray photoelectron spectroscopy (XPS). As shown in Fig. 2a, the bonding energy of V $2p_{3/2}$ (517.3 eV) and V $2p_{1/2}$ (524.6 eV) peaks has no significant changes in the two samples, and the valence state of V is +4.

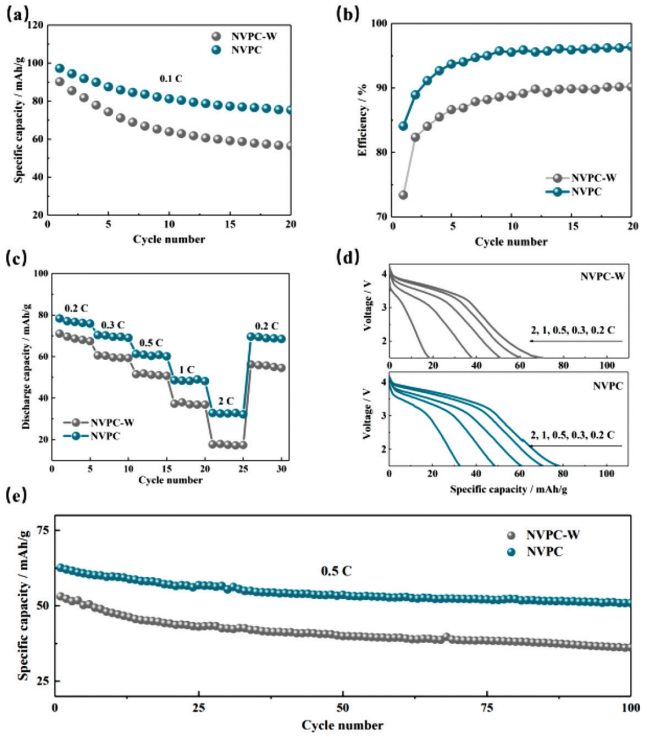

Fig. 3. Electrochemical performance of the materials. (a) Discharge capacity of the materials at 0.1 C. (b) Coulombic efficiency of the materials at 0.1 C. (c) Rate performance and (d) the corresponded charge/discharge profiles of the materials from 0.2 C to 2 C. (e) Cycling performance at 0.5 C.

The C–O bond and C=O bond that derived from the (C_2O_4) group are identified in the C 1s spectra (Fig. 2b) [34]. As the C 1s profiles of the NVPC-W and NVPC are similar, the bonding structure that associated with the (C_2O_4) group keeps stable after crystal water elimination. The same phenomenon is also observed in the O 1s and P 2p spectra (Fig. S1 in Supporting information). Morphology of the NVPC-W and NVPC were investigated by scanning electron microscopy (SEM). Both of the two samples demonstrate uniform micron scale plate-like shapes (Figs. 2c and d, Fig. S2 in Supporting information). These observations verify the topologic process of the crystal water removal, which shows negligible influence on physiochemical properties of materials. Chemical contents and distributions of the NVPC was further examined by elemental mapping (Figs. 2e and f). The atomic ratio of Na:V:P (5.50%:5.69%:5.76%) is close to the theoretical ratio in NVPC phase. Besides, it can be observed that the O, Na, V, P, C elements are evenly distributed, indicating high purity of the NVPC material.

After checking the physiochemical properties, we then cast our eyes over the electrochemical performance of the materials in sodium-ion batteries. As shown in Fig. 3a, the initial discharge capacity of the NVPC-W and NVPC is 90.2 mAh/g and 97.3 mAh/g, respectively, but the capacity of NVPC-W decreases very fast. After 20 cycles at 0.1 C (1 C = 100 mA/g), the discharge capacity of NVPC-W decreases to 56.5 mAh/g, while 75.3 mAh/g remains in the NVPC. The low Coulombic efficiency (CE) in NVPC-W should be a key reason for the fast capacity loss. As shown in Fig. 3b, the initial Coulombic efficiency (ICE) of NVPC (84.09%) is much higher than the NVPC-W (73.40%). Besides, although the CE gradually increase as the cycling goes on, CE of the NVPC-W can only reach to around 90%. Such low CE is fatal to cycling stability. In the contrast, the CE in NVPC shows a substantial improvement, reaching to around 96%. Of note, the materials demonstrate a redox platform centered at around 3.8 V (Fig. S3 in Supporting information). Such a high voltage derives from the redox of V^{4+}/V^{5+}, which is verified by ex-situ XPS (Fig. S4 in Supporting information). Rate performance of the materials are shown in Figs. 3c and d. The NVPC can deliver discharge capacity of 78.4, 70.5, 61.3, 48.6 and 32.9 mAh/g at 0.2, 0.3, 0.5, 1 and 2 C, respectively. While the crystal water contained material shows inferior rate performance, with a discharge capacity of 71.1, 60.6, 51.4, 37.3 and 17.7 mAh/g at the corresponding C-rates. Of note, when the current turns back from 2 C to 0.2 C, 88.7% of the initial capacity can be obtained in NVPC, which is much higher than that of the NVPC-W (79.1%). Cycling stability of the materials was also studied. As shown in Fig. 3e, NVPC and NVPC-W exhibits a capacity retention of 81.4% and 68.0%, respectively, after 100 cycles at 0.5 C. Therefore, the existence of crystal water does have fundamental influence on electrochemical performance of the materials.

The poor CE and rate performance of NVPC-W implies that existence of crystal water is negative for the electrode reaction kinetics. Because the crystal water molecules occupy the lattice vacancies of NVPC-W, it may affect sodium diffusion and limit sodium accommodation, thus leading to sluggish reaction kinetics. To verify this hypothesis, cyclic voltammetry (CV) was used to study the reaction kinetics of the NVPC-W and NVPC electrodes. Based on the Randles Sevchik equation [35,36]:

$$I_p = 2.69 \times 10^5 n^{\frac{3}{2}} A C_0 D_{Na}^{\frac{1}{2}} v^{\frac{1}{2}} \quad (1)$$

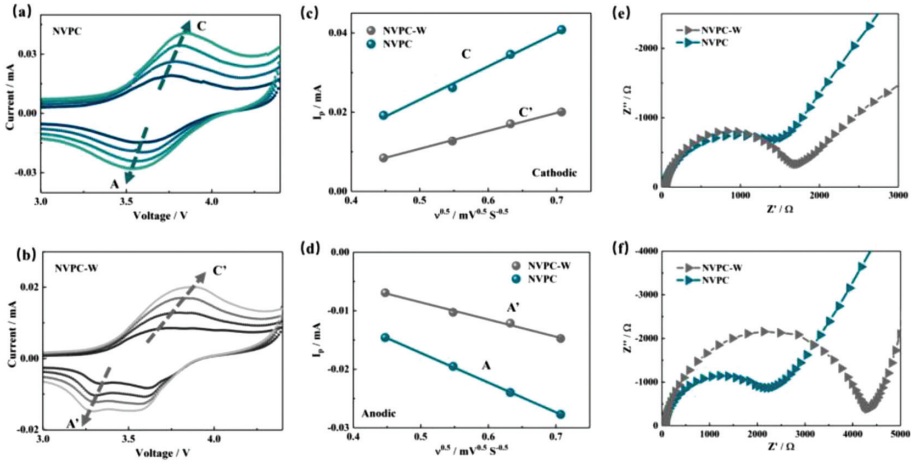

Fig. 4. Kinetics analysis. (a) CV plots of the NVPC and (b) NVPC-W at different scan rate from 0.2 mV/s to 0.5 mV/s. (c) The I_p–$v^{0.5}$ plots in cathodic and (d) anodic processes. (e) EIS plot of the fresh electrodes and the electrodes after 100 cycles at 0.5 C.

where n, A, C_0, D_{Na} and v represent the number of electrons transferred, surface area of the electrode, concentration of Na, apparent sodium diffusion coefficient, scan rate, and value of peak current. D_{Na} is proportional to the slope of fitting straight–line of I_p-$v^{0.5}$. CV curves of the two electrodes at different scan rates are depicted in Figs. 4a and b, and the corresponded fitting results of I_p-$v^{0.5}$ plots are displayed in Figs. 4c and d. Obviously, the slopes of NVPC in both the cathodic and the anodic processes are larger than that of NVPC-W, indicating that the sodium diffusion kinetics is greatly enhanced in NVPC. Besides, the contribution of pseudocapacitance, another important parameter that associated with the rate performance of electrode materials [37] was also calculated based on CV. While it shows that the crystal water has little influence on the pseudocapacitance behavior (Figs. S5 and S6 in Supporting information). Therefore, kinetics is the key factor that determines rate performance of the NVPC-W and NVPC. Of note, the difference of CV curves between NVPC-W and NVPC, especially during the anodic process, may be accounted to the crystal water involved side reactions and the difference of electrode kinetics [38].

Apart from kinetics, stability of the electrodes is another issue that affects electrochemical performance [39]. In organic electrolyte systems, the crystal water in materials may trigger side reactions and generate HF, which greatly accelerates electrode degradation and reduces cycling stability of the materials [31,40,41]. To verify it, the NVPC-W and NVPC electrodes before and after cycling were investigated by electrochemical impedance spectroscopy (EIS). The equivalent circuit diagram is presented in Fig. S7 (Supporting information). As shown in Figs. 4e and f, a significant charge transfer resistance increase from 1651.2 Ω to 4269.5 Ω is observed in NVPC-W after the cycling. In the contrast, the charge transfer resistance increase is much smaller in NVPC (from 1450.3 Ω to 2119.7 Ω). Therefore, the elimination of crystal water is important to ensure the cycling stability of electrode.

In summary, the crystal water in the oxalate-phosphate NVPC-W material is proven feasibly to be removed by vacuum drying at 150 °C. The removal process shows no harm to physiochemical properties of NVPC, including the crystal structure, chemical bonding, and morphology. While the crystal water is found to fundamentally affect electrochemical performance of the materials, as the crystal water elimination enables substantial improvements of the NVPC material in terms of CE, rate, and cycling performance. It is suggested that the crystal water hinders sodium diffusion, limits its sodium accommodation, and damages electrode stability, leading to sluggish reaction kinetics and reduce cycling stability. The discoveries should be helpful to further develop advanced oxalate-phosphate electrode materials.

Declaration of competing interest

The authors declare no conflict of interest.

Acknowledgment

The authors thank the financial support from the National Key R&D Program of China (No. 2019YFC1908301).

Supplementary materials

Supplementary material associated with this article can be found, in the online version, at doi:10.1016/j.cclet.2022.107898.

References

[1] C. Vaalma, D. Buchholz, M. Weil, S. Passerini, Nat. Rev. Mater. 3 (2018) 18013.
[2] N. Yabuuchi, K. Kubota, M. Dahbi, S. Komaba, Chem. Rev. 114 (2014) 11636–11682.
[3] C. Delmas, Adv. Energy Mater. 8 (2018) 1703137.
[4] Y. Fang, J. Zhang, L. Xiao, et al., Adv. Sci. 4 (2017) 1600392.
[5] X. Xiang, K. Zhang, J. Chen, Adv. Mater. 27 (2015) 5343–5364.
[6] J.Y. Hwang, S.T. Myung, Y.K. Sun, Chem. Soc. Rev. 46 (2017) 3529–3614.
[7] H. Li, M. Xu, Z. Zhang, et al., Adv. Funct. Mater. 30 (2020) 2000473.
[8] Q. Ni, Y. Bai, F. Wu, C. Wu, Adv. Sci. 4 (2017) 1600275.
[9] H. Li, M. Xu, H. Long, et al., Adv. Sci. 9 (2022) 2202082.
[10] J. Kim, D.H. Seo, H. Kim, et al., Energy Environ. Sci. 8 (2015) 540–545.
[11] C.S. Park, H. Kim, R.A. Shakoor, et al., J. Am. Chem. Soc. 135 (2013) 2787–2792.
[12] H. Kim, C.S. Park, J.W. Choi, Y. Jung, Angew. Chem. 55 (2016) 6662–6666.
[13] H. Li, T. Jin, X. Chen, et al., Adv. Energy Mater. 8 (2018) 1801418.
[14] H. Gao, Y. Li, K. Park, J.B. Goodenough, Chem. Mater. 28 (2016) 6553–6559.
[15] W. Zhou, L. Xue, X. Lu, et al., Nano Lett 16 (2016) 7836–7841.
[16] J. Zhang, Y. Liu, X. Zhao, et al., Adv. Mater. 32 (2020) 1906348.
[17] H. Li, M. Xu, C. Gao, et al., Energy Storage Mater 26 (2020) 325–333.
[18] H. Yi, L. Lin, M. Ling, et al., ACS Energy Lett. 4 (2019) 1565–1571.
[19] T. Wang, W. Zhang, H. Li, et al., ACS Appl. Energy Mater. 3 (2020) 3845–3853.
[20] H. Kim, I. Park, S. Lee, et al., Chem. Mater. 25 (2013) 3614–3622.
[21] H. Li, C. Guan, J. Zhang, et al., Adv. Mater. 34 (2022) 2202624.
[22] J. Kim, G. Yoon, M.H. Lee, et al., Chem. Mater. 29 (2017) 7826–7832.
[23] R. Zhang, H. Chen, H. Yue, Chin. Chem. Lett. 34 (2023) 107580.
[24] A.S. Hameed, M.V. Reddy, B.V.R. Chowdari, J.J. Vittal, Electrochim. Acta 128 (2014) 184–191.
[25] A.S. Hameed, M.V. Reddy, M. Nagarathinam, et al., Sci. Rep. 5 (2015) 16270.
[26] H. Xu, Q. Yan, W. Yao, et al., Small Struct 3 (2022) 2100217.
[27] Y. Yuan, Q. Wei, S. Yang, et al., Energy Storage Mater. 50 (2022) 760–782.
[28] T. Jin, H. Li, K. Zhu, et al., Chem. Soc. Rev. 49 (2020) 2342–2377.
[29] J. Song, L. Wang, Y. Lu, et al., J. Am. Chem. Soc. 137 (2015) 2658–2664.
[30] J.F. Colin, T. Bataille, S.E. Ashbrook, et al., Inorg. Chem. 45 (2006) 6034–6040.
[31] H. Li, W. Zhang, K. Sun, et al., Adv. Energy Mater. 11 (2021) 2100867.
[32] S.F. Lux, I.T. Lucas, E. Pollak, et al., Electrochem. Commun. 14 (2012) 47–50.
[33] M. Ohara, A.S. Hameed, K. Kubota, et al., Chem. Sci. 12 (2021) 12383–12390.
[34] H. Li, C. Guan, M. Xu, et al., Energy Storage Mater. 47 (2022) 526–533.
[35] W. Deng, X. Feng, Y. Xiao, C. Li, ChemElectroChem 5 (2018) 1032–1036.
[36] R. Zhang, Y. Zhang, K. Zhu, et al., ACS Appl. Mater. Interfaces 6 (2014) 12523–12530.
[37] H. Li, W. Zhang, Z. Han, et al., Mater. Today Energy 21 (2021) 100754.
[38] W. Wang, Y. Gang, J. Peng, et al., Adv. Funct. Mater. 32 (2022) 2111727.
[39] C. Gao, Q. Dong, G. Zhang, et al., ChemElectroChem 6 (2019) 1134–1138.
[40] H. Yi, R. Qin, S. Ding, et al., Adv. Funct. Mater. 31 (2020) 2006970.
[41] C. Duan, Y. Meng, Y. Wang, et al., Inorg. Chem. Front. 8 (2021) 2008–2016.